

OPEN ACCESS

The Role of Surface Free Energy in Binder Distribution and Adhesion Strength of Aqueously Processed $\text{LiNi}_{0.5}\text{Mn}_{1.5}\text{O}_4$ Cathodes

To cite this article: Andreas Weber *et al* 2024 *J. Electrochem. Soc.* **171** 040523

View the [article online](#) for updates and enhancements.

You may also like

- [Measurement of Adhesion Strength in Copper Interconnection Layers](#)
Tohru Hara, Minoru Uchida, Masayo Fujimoto *et al.*
- [Optimization of cold spray process parameters to maximize adhesion and deposition efficiency of Ni+Al₂O₃ coatings](#)
Oleksandr Shorinov, Anatolii Dolmatov, Sergii Polyvianny *et al.*
- [Enhanced adhesive strength between SU-8 photoresist and titanium substrate by an improved anodic oxidation method for high aspect-ratio microstructures](#)
Liyan Lai, Yunna Sun, Hao Wu *et al.*



Your Lab in a Box!

The PAT-Tester-i-16: All you need for Battery Material Testing.

- ✓ All-in-One Solution with integrated Temperature Chamber!
- ✓ Cableless Connection for Battery Test Cells!
- ✓ Fully featured Multichannel Potentiostat / Galvanostat / EIS!

www.el-cell.com +49 40 79012-734 sales@el-cell.com

EL-CELL[®]
electrochemical test equipment





The Role of Surface Free Energy in Binder Distribution and Adhesion Strength of Aqueously Processed $\text{LiNi}_{0.5}\text{Mn}_{1.5}\text{O}_4$ Cathodes

Andreas Weber,^z  Noah Keim,  Andreas Gyulai,  Marcus Müller,  Francesco Colombo, 
Werner Bauer,  and Helmut Ehrenberg 

Karlsruhe Institute of Technology - Institute for Applied Materials - Energy Storage Systems (IAM-ESS), 76021 Karlsruhe, Germany

This study identifies the critical aspects of binder distribution and mechanical integrity in aqueously processed LNMO cathodes, employing a comprehensive approach involving surface characterization techniques, adhesion strength testing, and electrochemical characterization. The investigation includes the use of the Washburn and Sessile Drop methods for surface free energy analysis, revealing key insights into the interfacial free energy of adhesion between cathode constituents. The results explain the formation of carbon-binder-domains and their impact on adhesion strength, with a particular focus on the conductive additives' (CA) surface area. The study demonstrates the effectiveness of reducing CA surface area and employing alternative conductive additives, such as vapor-grown carbon fibers (VGCF), in improving adhesion strength and mitigating capacity fade attributed to delamination during cycling. Furthermore, the research emphasizes the role of heat treatment beyond the melting point of the polyvinylidene fluoride (PVDF) latex binder, showcasing its influence on wetting and enhancing mechanical integrity. The presented methodology provides a valuable tool for predicting and optimizing binder distribution, offering insights into improving the overall performance and reliability of aqueously processed cathodes for advanced lithium-ion batteries.

© 2024 The Author(s). Published on behalf of The Electrochemical Society by IOP Publishing Limited. This is an open access article distributed under the terms of the Creative Commons Attribution 4.0 License (CC BY, <http://creativecommons.org/licenses/by/4.0/>), which permits unrestricted reuse of the work in any medium, provided the original work is properly cited. [DOI: 10.1149/1945-7111/ad3a24]



Manuscript submitted February 9, 2024; revised manuscript received March 28, 2024. Published April 16, 2024.

Supplementary material for this article is available [online](#)

N-Methyl-2-pyrrolidone (NMP) as solvent for homogeneous and stable slurries still represents the current state-of-the-art in the manufacturing of cathodes for lithium ion batteries (LIB).¹ It delivers a good PVDF solubility, which is a wide-spread binder owing to its high electrochemical stability, its good dispersion quality in the slurry as well as a favorable wettability with electrolyte.²⁻⁴ The downside to NMP, however, is its high cost and its reproductive toxicity which entails the classification as a CMR (carcinogenic, mutagenic and toxic to reproduction) substance. Water as alternative solvent has increasingly moved into the focus of electrode slurry preparation over the last decade as it is not only more environmentally friendly but also offers significantly lower material costs.⁵ Due to a rise in environmental awareness covering issues such as recycling, waste gas treatment and work safety classical NMP-based and aqueously processed cathodes increasingly differ from an economical point of view.⁶ As stated by Liu et al. solvent recovery alone accounts for approximately 47% of the overall energy consumption and nearly 5% of the LIBs cost.¹ Considering negative electrodes, their suitability for water-based processing and resulting performance has already been extensively evaluated and water-borne anodes have been established in industrial scale manufacturing for over a decade.^{1,5} However, water-borne cathodes still suffer from a broad variety of issues such as poor paste homogeneity and agglomeration effects, corrosion of the current collector due to high pH values as well as aging of the active materials when exposed to water or even moisture.⁷⁻⁹ In the past, studies on water-based slurries for Li-ion cathode manufacturing primarily investigated the industrially well-established active materials such as lithium iron phosphate (LFP), lithium cobalt oxide (LCO), lithium nickel cobalt aluminum oxide (NCA) and lithium nickel manganese cobalt oxide (NMC).^{5,10-13} Regarding the application of lithium nickel manganese oxide ($\text{LiNi}_x\text{Mn}_y\text{O}_4$, LNMO) in water-borne cathodes, there still exists a deficit of knowledge and experience. LNMO offers a multitude of excellent properties as an active material for positive electrodes as for example a theoretical capacity of 147 mAh/g and a nominal cell voltage of 4.7 V (vs

Li^+/Li). Furthermore, it can be fully delithiated and lithiated while charging and discharging without suffering significant structural damage.¹⁴ Based on realistic graphite full cell capacities of 120 mAh/g for LNMO its specific energy density is highly competitive compared to current state-of-the-art active materials such as and $\text{LiNi}_{0.6}\text{Co}_{0.2}\text{Mn}_{0.2}\text{O}_2$ (NMC 622) and $\text{LiNi}_{0.8}\text{Co}_{0.1}\text{Mn}_{0.1}\text{O}_2$ (NMC 811). With up to 464 Wh/kg LNMO surpasses both NMC 622 and NMC 811 delivering 416 Wh/kg and 448 Wh/kg, respectively.¹⁵ LNMO offers further advantages as it is free of cobalt and utilizes the nickel redox capacity in its entirety, resulting in cost savings up to 50% at material and 10%–20% at cell level.¹⁶ The desired high potential of LNMO (up to 5.0 V vs Li/Li^+) does not come without challenges for the materials in use. Regarding the conductive additive, the limited stability of carbon blacks at voltages beyond 4.5 V and their influence on instable CEI formation in LNMO full cells was demonstrated by multiple authors.¹⁷⁻²¹ In respect of the binder, the focus of this work will be on using a combination of PVDF and CMC as binding agents as they are reported to offer good electrochemical stability in the voltage window of interest for this work.^{22,23} Further, the usage of CMC was demonstrated to have a beneficial impact on the rheological properties of aqueous slurries.²⁴ The PVDF under investigation comes as latex, a suspension of colloidal PVDF particles stabilized in water, which allows for the application of the non-water soluble PVDF in aqueous processing. Even so, water-based systems including the aforementioned binders frequently suffer from low mechanical integrity on both cathode²⁵⁻²⁸ as well as anode side²⁸⁻³⁰ regardless of the active material in use. An in-depth understanding of wetting and adhesion and their underlying principle, the surface free energy (SFE), is crucial for many industrial processes such as applying paint or ink on a surface,^{31,32} lubricating surfaces,³¹ detergent formulation^{33,34} or adhesive joining.³⁵ The latter is of particular interest for this work as the polymer binders in the electrode function as the adhesives. Investigation of the SFE therefore offers a promising foundation for optimizing the mechanical integrity of aqueously processed cathodes. This study is showcasing two methods for characterizing the SFE of frequently applied materials in electrode manufacturing and understanding the driving forces behind binder distribution in aqueous systems. The

^zE-mail: andreas.weber@kit.edu

final objective of this work is the comparison of cathodes manufactured using different conductive additives and testing adhesion strength and cycle life while maintaining the same energy density throughout the electrodes.

Experimental

Surface free energy measurements.—Each individual cathode component as listed in Table III was tested either using the Washburn (WB)^{36–38} or the Sessile Drop (SDP)³⁹ measurement. The choice of method being dependent upon the feasibility of creating a sample with a dense surface without changing its surface chemistry. Both of the conductive additives (CA) (C-ENERGY Super C65, specific surface area (S) = 62 m²/g, Imerys Graphite & Carbon, Switzerland and VGCF-H, S = 12 m²/g, Resonac Corporation, Japan) as well as the LNMO (S = 0.29 m²/g, Haldor Topsoe, Denmark) were measured by WB method on a force tensiometer (K100, Kruss Scientific, Germany) as it was not possible to achieve closed surfaces able of holding liquid drops. Both polymer binders could not be measured by the WB method as they clogged the pores of the filter fixed to the bottom of the testing capillary preventing the rise of the probing liquids. The PVDF latex (Kynar) (solid content = 31 wt%, particle size = 213 nm) was received from Arkema (France). It was consequently pressed into a pellet with a diameter of 14 mm by applying a nominal load of 500 kPa after drying at 50 °C under vacuum. The CMC (Walocel CRT 2000 PA 07, DuPont, USA) was coated with a thickness of approximately 20 μm onto a glass substrate. The measurement of the aluminum foil was performed on a 14 mm circular punch-out. The contact angle was subsequently determined according to the SDP method using a DSA25E (Kruss Scientific, Germany).

The reference measurement of the capillary constant was performed using n-hexane as fully wetting liquid for all samples measured by WB method. γ_L is the liquid surface tension. γ_L^d and γ_L^p are the dispersive and polar components of surface free energy. The physicochemical properties of the applied probing liquids are given in Table I.

Electrode manufacturing.—The different electrodes slurries were prepared by disc agitation (Dispermat, VMA Getzmann, Germany) of LNMO, the conductive additive, CMC, an experimental PVDF latex and deionized water. They were then coated onto

an 18 μm thick aluminum current collector by doctor blade at a line speed of 0.2 m/min and dried in-line at 25 °C under circulating air, which makes it possible to dry the electrode before a detectable onset of corrosion, using a role-to-role coating line (KTFS, Mathis AG, Switzerland). The electrodes were subsequently calendered at 50 °C (GKL200, Saueressig, Germany) to a porosity of 30%. The formulations of the different cathodes and the respective active material loadings are summarized in Table II.

Anodes for full cell testing were prepared with 96 wt% graphite (SMG-A3, Hitachi, Japan), 1.5 wt% CB (C-ENERGY Super C65, Imerys Graphite & Carbon, Switzerland), 1.25 wt% CMC (Walocel CRT 2000 PA, DuPont, USA), and 1.25 wt% styrene-butadiene rubber (SBR) (TRD 2001, JSR Micro, Belgium) and were coated onto copper foil with a thickness of 10 μm. The loading was set to 2.2 mAh/cm². By calendering the porosity was set to 48%.

Adhesion strength testing.—Using a zwickiLine Z2.5/TN (ZwickRoell, Germany), the adhesion strength of the coatings before and after calendaring at 50 °C (GKL200, Saueressig, Germany) and 175 °C (GK300L, Saueressig, Germany) as well as after annealing in a convection oven at 175 °C ($T_{\text{melt PVDF}} = 163$ °C) for 10 and 40 min was measured in a 90° peel test. The samples were prepared by fixing 60 mm × 17 mm electrode stripes to a double-sided adhesive tape with the coating facing downwards to a metallic holder and pressed with a load of 0.3 MPa for 10 s. The aluminum foil was then peeled off from the electrode layer at a constant speed of 60 mm/min in a 90° angle. The adhesion strength in N/m was determined through a 10 N load cell and evaluated as mean value on a peel length of 40 mm dismissing the data gathered on the first and last 10 mm of the test.

Resistivity measurements.—Both interface and bulk resistivity were simultaneously measured on a Hioki RM2610 based on the finite volume method (FVM). Measurements were repeated five times for each cathode. Measuring points were chosen at random.

SEM and EDS analysis.—SEM micrographs were taken using a Gemini (Carl Zeiss, Germany) at an acceleration voltage of 2 kV. EDS analysis was carried out with an Ultim Extreme Detector (Oxford Instruments, UK) at an acceleration voltage of 4 kV. Cross sections were prepared by ion milling on a TIC3X (Leica Microsystems, Germany).

Cell assembly.—Cells were built from the coatings that were calendered at 50 °C and annealed at 175 °C for 40 min. Foregoing the assembly of the cells, the electrodes were dried again at 110 °C for 4 h in a vacuum oven to evaporate residual water. Coin cells with a graphite anode were built inside an argon filled glove box with both electrodes having a diameter of 12 mm, a glass fiber separator (Whatman GF/C, Sigma-Aldrich, USA) and 200 μl of LP30 (1:1 EC/DMC, 1 M LiPF₆, Sigma-Aldrich, USA) containing 1 wt% of lithium bis(oxalato)borate (LiBOB, Sigma-Aldrich, USA) and tris(trimethylsilyl) phosphite (TMSP, Sigma-Aldrich, USA) each. After manual assembly the cells were pressed with a nominal force of

Table I. Physicochemical properties of probing liquids at 20 °C³⁷.

Probing liquid	ρ (g/ml)	η (mPa·s)	γ_L	γ_L^d (mJ/m ²)	γ_L^p
n-Hexane	0.661	0.326	18.4	18.4	0.0
Water	0.998	1.000	72.8	21.8	51.0
Diiodomethane (DIM)	3.325	2.762	50.8	50.8	0.0
Dimethyl Sulfoxide (DMSO)	1.100	1.996	44.0	36.0	8.0
Ethylene glycol	1.109	21.81	48.0	29.0	19.0

Table II. Cathode compositions.

Reference	LNMO	CMC	PVDF (wt%)	CA	Type of CA	Areal capacity (mAh/cm ²)
C65 _{0.0wt%}	95.2	1.9	2.9	0.0	—	2.00
C65 _{1.4wt%}	93.9	1.9	2.8	1.4	C65	2.05
C65 _{2.8wt%}	92.6	1.8	2.8	2.8	C65	2.02
C65/VGCF _{1.4+1.4wt%}	92.6	1.8	2.8	1.4 + 1.4	C65 + VGCF	1.91
VGCF _{2.8wt%}	92.6	1.8	2.8	2.8	VGCF	1.87
C65/VGCF _{norm.}	94.12	1.19	1.85	1.42 + 1.42	C65 + VGCF	1.98
VGCF _{norm.}	95.68	0.56	0.87	2.89	VGCF	1.85

5.2 MPa for 10 s. To check reproducibility, three coin cells with a N/P ratio of 1.1 were built and tested for each coating.

Cell cycling and rate capability.—The assembled cells rested for 48 h prior to the electrochemical testing to assure full wetting of all components inside the cells by the electrolyte. Rate capability and long-term cycling tests were performed at 25 °C within a voltage interval of 3.5 V–4.9 V vs Li/Li⁺, assuming 147 mAh/g as specific capacity of LNMO.

Starting with the initial formation of the cells, three cycles at 0.1 C (charge/discharge) were performed. Rate capability was then tested according to the following charge/discharge pattern: 0.5 C/0.5 C; 0.5 C/1 C; 0.5 C/2 C; 0.5 C/5 C; 0.5 C/10 C for 5 cycles each and 100 cycles at 0.5 C/1 C (charge/discharge) with every 20th cycle at 0.2 C (charge/discharge). Charging of the cells consisted of a constant current mode up to 4.9 V and a subsequent constant voltage step with 0.05 C as cut-off limit (constant current—constant voltage (CCCV)).

Formation of the cells for long-term cycling was carried-out as mentioned above. The cells were then cycled for 1000 cycles at 0.5 C/1 C (charge/discharge). Every 50th cycle a C-rate of 0.1 C/0.1 C was applied. CCCV charging as described above was also used in long-term cycling.

Tortuosity by EIS.—Tortuosity was measured in a symmetrical cell configuration. Three coin cells were built for each coating that had undergone calendaring at 50 °C and annealing at 175 °C for 40 min consisting of two cathodes with a diameter of 16 mm, a trilayer PP/PE/PP separator (H2013, Celgard, USA) and an electrolyte with non-intercalating conditions, namely EC:DMC (1:1 vol: vol) with 0.01 M tetrabutylammonium perchlorate (TBAClO₄, Sigma Aldrich, >99.0%).

Potentiostatic impedance spectra were obtained across a frequency range of 100 kHz to 20 mHz. The measurement was repeated

50 times with an OCV step of one hour between individual measurements. The equivalent circuit model applied for fitting the data is illustrated in Fig. S1.

Results and Discussion

Mechanical properties.—The resulting adhesion strength as depicted in Fig. 1 show poor mechanical integrity for all coatings containing a CA amount of 2.8 wt% in their uncalendered state. While calendaring at 50 °C with a roll speed of 1 m/min leads to an improvement in adhesion strength by approx. 100% for most coatings, C65_{2.8wt%} exhibits only slightly enhanced adhesion. The melting temperature of the PVDF is stated to be at 163 °C by the manufacturer. Hot calendaring at 175 °C with a roll speed of 1 m/min shows an additional improvement in adhesion strength. However, the most significant rise in the mechanical strength of the electrodes can be observed with annealing of the coatings at 175 °C after the calendaring step which reaches a plateau after a duration of 40 min. All coatings containing CB show a lesser increase in adhesion strength compared to coatings C65_{0.0wt%} and VGCF_{2.8wt%} when exposed to heat treatment for only 10 min. However, longer exposure time of 40 min yields results comparable to that of VGCF_{2.8wt%}. Regarding C65_{2.8wt%}, the heat treatment, irrespective of its duration, has an insignificant impact on adhesion strength. The adhesion strength of a PVDF (Solef 5130, Solvay, France) cathode calendared to 30% porosity with a binder content of 4.6 wt% manufactured in the conventional organic solvent (NMP) based process is given by the dashed red line.

The low surface area VGCF have a slightly negative effect on the mechanical strength of the cathode, since a drop from 72.9 N/m for C65_{1.4wt%} to 67.5 N/m for C65/VGCF_{1.4+1.4wt%} was measured for heat treated samples. Nevertheless, the influence of VGCF on the adhesion is substantially smaller than that of the high surface area C65, as adhesion strength for C65_{2.8wt%} was measured to be only

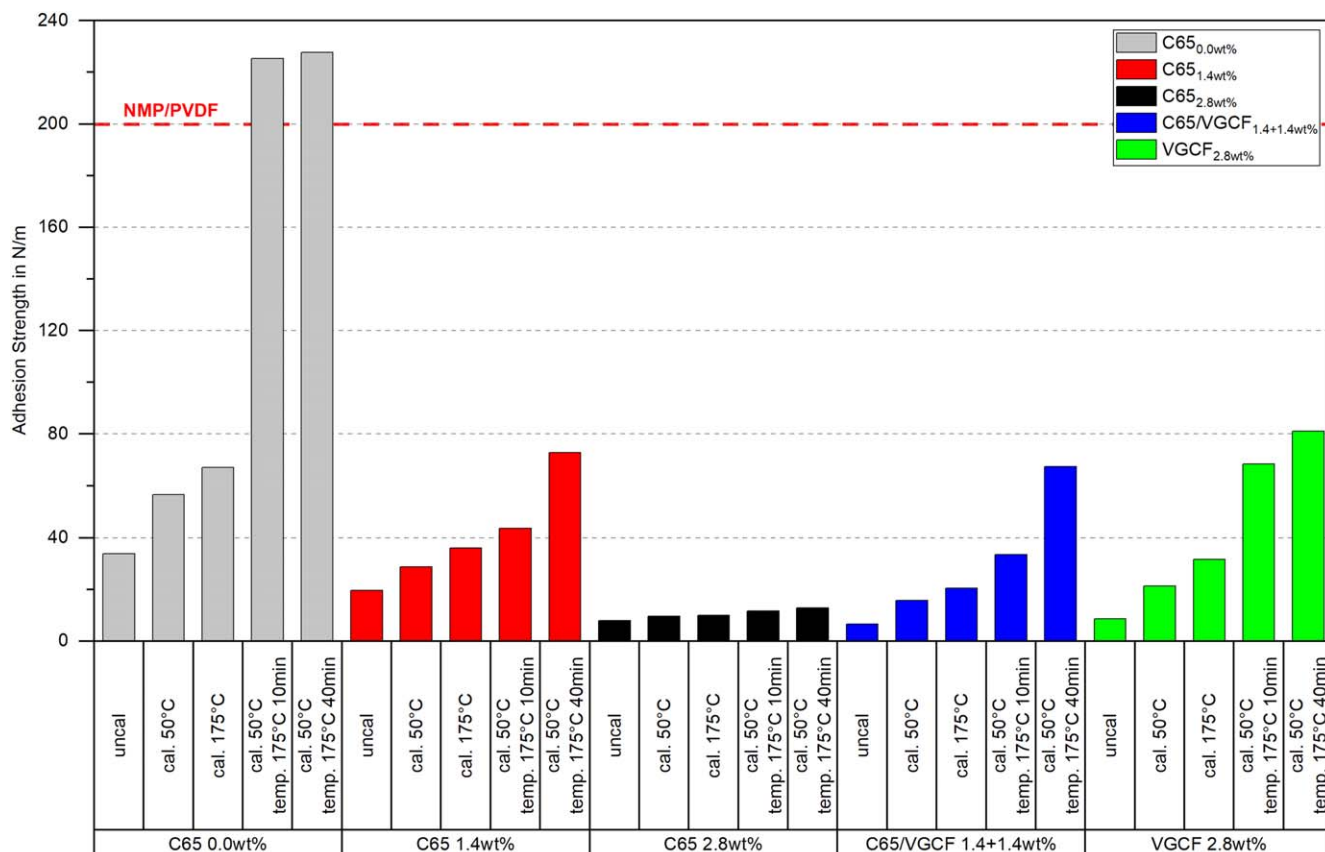


Figure 1. Adhesion Strength of uncalendered, calendared and heat-treated cathodes.

Table III. Contact angle measurements of electrode components \pm standard deviation, $n = 3$.

Solid sample	n-Hexane Capillary constant	Water	DIM	DMSO Contact angle (degrees)	EG	Method
C65	$1.7 \cdot 10^{-5}$	89.6 ± 0.4	64.4 ± 1.0	38.7 ± 0.6	—	WB
VGCF	$2.0 \cdot 10^{-5}$	90.0 ± 0.1	80.9 ± 0.5	80.0 ± 3.7	—	WB
LNMO	$3.4 \cdot 10^{-6}$	42.9 ± 1.5	61.3 ± 0.5	2.8 ± 0.1	—	WB
CMC	n/a	—	38.5 ± 2.1	17.0 ± 1.8	9.4 ± 0.2	SDP
PVDF	n/a	69.1 ± 0.4	44.2 ± 0.3	—	37.4 ± 0.5	SDP
Aluminum CC	n/a	85.2 ± 1.0	47.5 ± 2.2	—	62.0 ± 0.1	SDP

12.9 N/m even though the amount of CA is the same as in C65/VGCF_{1.4+1.4wt%}.

The ability of the binder to bind the various solid components together is crucial in generating the required mechanical integrity for an electrode. With PVDF being present as latex and not in a dissolved state in aqueous processing, heat treatment above the binder's melting point becomes necessary. PVDF as a semi-crystalline polymer tends to be leathery to brittle below the melting temperature depending on its molar mass. In its molten state PVDF exhibits a lower viscosity which results in an increased wetting of the other solid components inside the cathode.³⁸ Thus, the mechanical integrity of the cathode is improved not only by an enlarged contact area due to wetting but also the mechanical interconnecting of PVDF with the solid components as liquid PVDF will flow into clefts and gaps and then solidify.

To distinguish between the effect of the differing surface areas and the effect of different surface chemistries of the CAs on adhesion strength and the binder distribution, coatings C65/VGCF_{norm.} and VGCF_{norm.} were manufactured. Assuming a quantity of 100 g, the total surface area (A) of C65_{2.8wt%} is $A = 200.5 \text{ m}^2$. According to Eq. S1 the theoretical binder layer thickness of C65_{2.8wt%} was then calculated to be 13.5 nm. Binder contents in C65/VGCF_{norm.} ($A = 130.5 \text{ m}^2$) and VGCF_{norm.} ($A = 60.5 \text{ m}^2$) were normalized to match a theoretical binder layer thickness of 13.5 nm to allow for a comparison between the CAs irrespective of their surface area. The resulting electrode compositions of the normalized electrodes are

given in Table II with two decimal places to avoid rounding errors. Resulting adhesion strengths are depicted in Fig. 2.

Both cathodes with normalized binder/surface area ratio exhibit a drop when calendered at 50 °C. The decline after calendaring is accounted to the lateral stretching of the coatings due to differing elastic moduli between binder and aluminum. Meyer et al. demonstrated the decline to be particularly pronounced in the porosity range between 30% to 35%.³⁹ However, the mechanical integrity can be restored by annealing. With normalized binder content it becomes apparent that there is an influence of the type of CA in use. The maximum adhesion strength after heat treatment for 40 min ranges from 12.9 N/m for C65_{2.8wt%} to 15.6 N/m and 17.4 N/m for C65/VGCF_{norm.} and VGCF_{norm.}, respectively, illustrating a positive effect of VGCFs on the mechanical integrity beyond their smaller surface area.

Surface free energy.—Table III summarizes the results of the contact angle measurements of the tested cathode constituents with each of the aforementioned probing liquids while also listing the applied method. As the WB method relies on a preceding measurement of the sample powder's capillary constant, the values are also given. CMC was not measured with water as it dissolves therefore delivering unreliable contact angles.

Based on the Owens-Wendt-Rabel-Kaelble (OWRK) model^{40–42} the contact angles can be converted into the SFE of the individual electrode component as given in Table IV. In addition to the overall

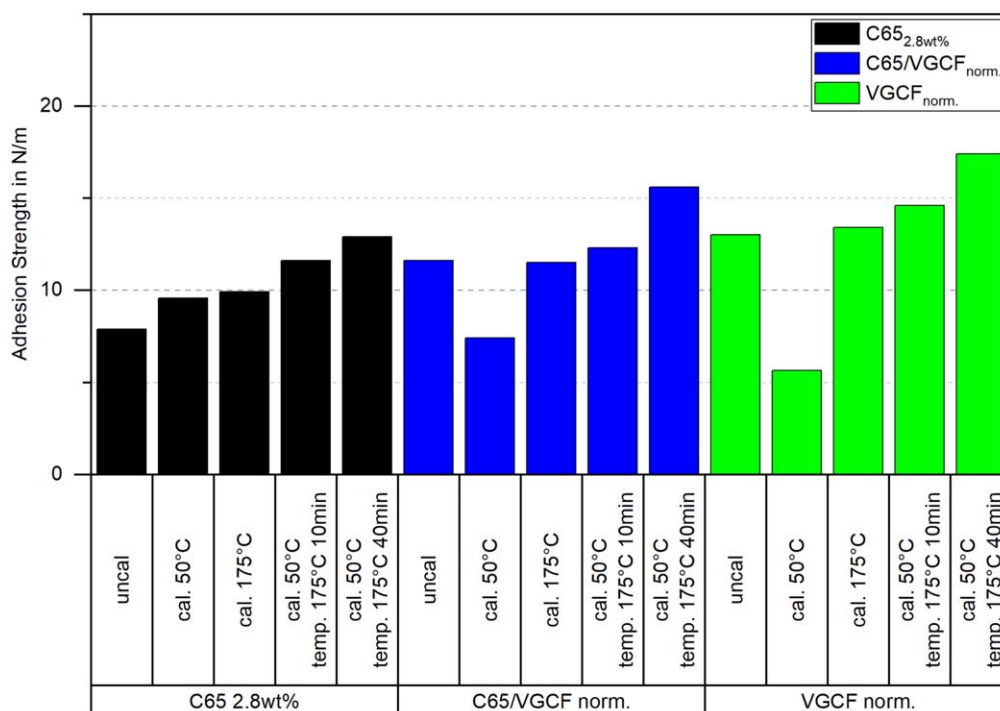
**Figure 2.** Adhesion Strength of cathodes with normalized binder contents.

Table IV. Surface free energy and free energy of adhesion of slurry components in relation to PVDF latex and CMC binder \pm standard deviation (ΔG_{132}^{IF} annotated as $\Delta G_{S-H_2O-PVDF}^{IF}$ and $\Delta G_{S-H_2O-CMC}^{IF}$ with 1 representing the solid sample s, 3 the immersion liquid H₂O and 2 the respective polymer binder).

Solid sample	γ_s	γ_s^d	γ_s^p (mJ/m ²)	$\Delta G_{S-H_2O-PVDF}^{IF}$	$\Delta G_{S-H_2O-CMC}^{IF}$
Aluminum CC	35.5 \pm 1.5	32.7 \pm 1.3	2.8 \pm 0.2	-48.5	-49.0
C65	31.7 \pm 1.2	28.6 \pm 1.0	3.1 \pm 0.2	-46.7	-47.1
CMC	47.3 \pm 1.5	38.5 \pm 1.2	8.8 \pm 0.4	-38.9	-39.7
PVDF Latex	44.2 \pm 1.0	35.4 \pm 0.9	8.8 \pm 0.2	-38.2	-38.9
VGCF	19.7 \pm 1.5	12.8 \pm 1.1	6.9 \pm 0.4	-34.9	-34.4
LNMO	55.6 \pm 1.1	25.6 \pm 0.9	30.0 \pm 0.2	-14.9	-15.1

SFE and both the dispersive γ_s^d and polar γ_s^p parts, the interfacial free energy of adhesion ΔG_{132}^{IF} is also compiled. As a result, the carbon black shows a significantly larger dispersive and only a small polar component, which is in good accordance with literature.⁴³⁻⁴⁶ The current collector exhibits SFE highly similar to C65. While the dispersive part still dominates for both binders, PVDF and CMC, the polar part is higher than that of CB. VGCF also shows a mainly dispersive SFE. However, the dispersive and polar components are far more similar to each other than for C65. LNMO exhibits, as the only constituent, a larger polar than dispersive component, which is in alignment with findings on other active material in literature.⁴⁶ According to van Oss et al.^{47,48} the interfacial free energy of adhesion ΔG_{132}^{IF} between two condensed-phase materials 1 and 2 fully immersed in a liquid 3 is given by:

$$\Delta G_{132}^{IF} = \Delta G_{132}^d + \Delta G_{132}^p \quad [1]$$

with

$$\Delta G_{132}^d = \gamma_{12}^d - \gamma_{13}^d - \gamma_{23}^d \quad [2]$$

or

$$\Delta G_{132}^d = \gamma_1^d + \gamma_2^d - 2\sqrt{\gamma_1^d \gamma_2^d} - \gamma_1^d - \gamma_3^d + 2\sqrt{\gamma_1^d \gamma_3^d} - \gamma_2^d - \gamma_3^d + 2\sqrt{\gamma_2^d \gamma_3^d} \quad [3]$$

Equations 2 and 3 having d as superscript are equally valid with superscript p. The resulting free energy of adhesion functions as a measure for the aspirations of two compounds submerged in a liquid to agglomerate/form an interface. Positive values of ΔG_{132}^{IF} indicate repulsion of the immersed particles and a stable dispersion while negative values show attraction and the tendency for the formation of interfaces.^{48,49}

The preferential order of adhesion for both binders can therefore be derived from the most negative value for the free energy of adhesion towards the least negative in the following manner: CC>C65>other binder>VGCF>LNMO. PVDF as well as CMC yield the most negative values for ΔG_{132}^{IF} of -48.5 mJ/m² and -49.0 mJ/m² with the aluminium current collector. Both binders can therefore be expected to preferably bind to the aluminium current collector as it is energetically most beneficial. It is followed by C65, indicating the formation of CBDs. ΔG_{132}^{IF} of both binders towards each other is -38.9 mJ/m². VGCFs display a ΔG_{132}^{IF} of -34.9 mJ/m² with PVDF and -34.4 mJ/m² with CMC. As both binders exhibit a higher tendency to coagulate then to form an interface with the VGCFs, homogeneity issues are to be expected when using VGCFs. Regarding LNMO, ΔG_{132}^{IF} results in -14.9 mJ/m² and -15.1 mJ/m² for PVDF and CMC, making it the least preferred binding partner inside the slurry for both polymer binders.

Binder distribution.—SEM images of electrode C65_{2.8wt%} (Figs. 3A/1 and 3A/2) reveal LNMO particles seemingly covered by carbon-binder-domains (CBD). Yet, the formation of large gaps

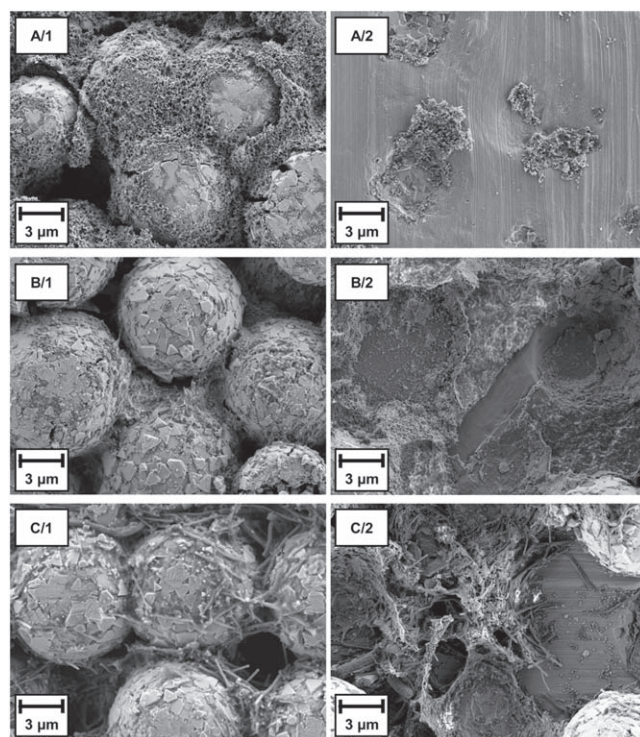


Figure 3. SEM micrographs for coatings C65_{2.8wt%} (A/1/2), C65_{0.0wt%} (B/1/2), VGCF_{2.8wt%} (C/1/2) after calendaring at 50 °C to 30% porosity and heat treatment at 175 °C for 40 min of top view (left) and current collector (right) after 90° peel tests.

between the active material particles and the CBD (Fig. 3A/1) hint at low adhesion of the binders towards the LNMO. Inspecting the current collector, it is found to be almost bare, with only few CBD remains adhering to the aluminum where LNMO particles have been pressed into the CC during calendaring. With reduced content of conductive additive to 0 wt% and 1.4 wt% a reduced gap formation as well as an improved coverage of the active material by the binder can be seen as depicted in Fig. 3B/1 and Fig. S2D/1, respectively.

Furthermore, the emergence of a thin coating layer on the CC can be observed, which was analyzed by EDS to consist of intermingled CMC and PVDF as illustrated in Fig. 4. The dark area in the upper left corner of all four elemental mappings are due to shadowing effects resulting from the installation angle of the EDS detector. Electrodes C65/VGCF_{1.4+1.4wt%} and VGCF_{2.8wt%} (Fig. S2E/2, and Fig. 3C/2) show no gap formation between the active material and the CBDs. Simultaneously they exhibit the coating film formation upon the CC even though the amount of CA in both coatings is identical to that of C65_{2.8wt%}.

SEM images of cross-sections prepared by ion-milling (Fig. 5A) further illustrate the poor adhesive behavior of the CBDs towards

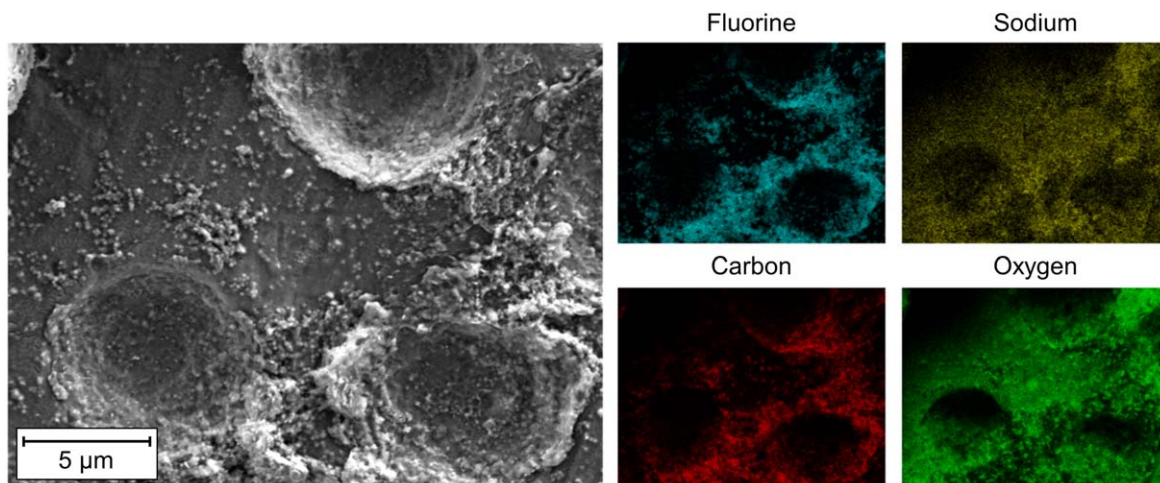


Figure 4. EDS analysis of current collector of electrode C65_{1.4wt%} after 90° peel test revealing formation of CMC/PVDF layer.

LNMO as the large gap formation can be observed throughout the entire thickness of electrode C65_{2.8wt%} with some active material particles laying seemingly contactless between the CBDs. Moreover, delamination of the coating from the CC was discovered (Fig. 5A). With reduction of the CA as well as the partial substitution of CB by VGCF improved adhesion of the binders towards LNMO becomes evident. Active material particles are fully covered by CMC and PVDF when no CA is present in the coating (Fig. 5B). C65/VGCF_{1.4+1.4wt%} indicates an improved coverage of LNMO by the binders as seen in Fig. 5C. However, gap formation can still be observed to a lesser extent. In addition to the improved covering of the active material, delamination does not occur with both lesser CA content and CB substitution. The predicted homogeneity issues due to both binders preferably coagulating rather than binding onto the VGCF, can be evidenced throughout electrode C65/VGCF_{1.4+1.4wt%} in the form of non-deagglomerated VGCF clusters.

It has been found that due to comparably low interfacial surface tensions between both polymeric binders and C65 the preferred formation of carbon-binder-domains can be expected, as evidenced by Fig. 3A/1. The calculation of ΔG^{IF} further supports the unfavored interaction of LNMO with both binders.⁵⁰ Owing to this deficit of attraction the CBDs solely disperse around the active material while not properly adhering to its surface.^{50,51} It is well reported in literature^{52,53} that when in contact with particle surfaces of the active material or the conductive additive the polymers will display the tendency to either adsorb or chemically bond to these surfaces aligning their chain ends with the surface and thus forming a bound polymer layer. By interaction with neighboring polymer layers, the polymer chains lose their mobility resulting in fixed/immobilized layers. Unbound polymer domains only start to form once a saturation of fixed polymer layers on the surface of the conductive additive and the active material is reached. As seen in Fig. 3A/1 the vast majority of binder polymers is fixed inside the CBDs due to the high affinity of both binders towards C65 and the CAs significantly large surface area within the electrode. The free binder domains are, however, substantial for maintaining both the cohesive as well as the adhesive integrity of the electrode.^{52,54,55}

While the aluminum CC acts as an even more preferred surface to the binders than the CB, the overall process of cathode manufacturing has to be kept in mind. While CMC, PVDF and CB undergo the dispersing by a disc agitator during the preparation of the slurry, the CC only comes into contact with both binders during the subsequent casting. In this sequence the polymeric binders are already in an immobilized state leaving only a miniscule fraction of free binder to form an adhesive bond towards the CC. A reduction of the CA's surface area therefore leads to a faster saturation of the CA by the binder and the formation of free polymer domains, which will then

tend to bind onto the current collector as expected and evidenced by Fig. 4. The differently pronounced improvements in adhesion strength, shown in Fig. 1, can be explained by the free energy of adhesion and the resulting binder distribution. Regarding C65_{2.8wt%} the majority of both binders is immobilized inside the CBDs. Therefore, heat treatment beyond T_{melt} leads only to additional wetting of CB. For C65_{0.0wt%} and VGCF_{2.8wt%} the heat treatment at T_{melt} for 10 min was sufficient to reach the maximum adhesion strength, as PVDF was able to directly wet the active material particles and the current collector in the absence of C65. In electrodes C65_{1.4wt%} and C65/VGCF_{1.4+1.4wt%} PVDF does, in its molten state, initially wet CB. With longer exposition to temperatures above T_{melt} PVDF proceeds to also wet LNMO and the CC as evidenced in Fig. 1. The improved coverage of the active material in the absence of C65 as well as the observed coating layer on the CC (Fig. 4) are also evidenced by an increase in bulk and interface resistivity (Fig. 6).

Electrochemical characterization.—Rate capability tests from 0.5 C up to 10 C in Fig. 8 reveal inferior performance of the cathodes containing a reduced amount of conductive additive. It was not possible to cycle C65_{0.0wt%}. Tortuosity of the cells, depicted in the left graph of Fig. 7, increases with reduced total surface area of the CA, due to an excess amount of free binder.⁵⁶ The equation used to calculate the theoretical binder layer thickness of each individual cathode is given as Eq. S1.⁵⁷ Nevertheless, rate performances of the cathodes show no correlation with the tortuosity. However, they correspond well with both bulk and interface resistivity of the coatings (Fig. 6). This can be explained by an increased overpotential during charging as well as discharging due to the heightened electrical resistivity. Ultimately leading to an incomplete sequence of redox reactions in the chosen voltage window of 3.5 V–4.9 V vs Li/Li⁺. While it cannot be determined whether bulk or interface resistivity is the dominant limitation of C-rate performance it can be said that overall electrical resistivity demonstrates to be the limiting factor of C-rate performance at the examined porosity and loadings. The bulk and interface resistivity of coating C65_{1.4wt%} after calendaring and annealing could not be determined as it was out of the upper measuring limit of the Hioki resistance meter.

As illustrated in the right plot in Fig. 8 the initial capacity retention of the aforementioned electrodes is very similar. After approx. 500 cycles however, C65_{2.8wt%} starts exhibiting a continuously increasing sharp degradation. With every 50th cycle performed at a C-rate of 0.1 C/0.1 C (charge/discharge) it can be deduced that the loss in capacity is not mainly a result of active material degradation as a discharge capacity comparable to all other cathodes is achieved when charging at a low C-rate. It is therefore concluded

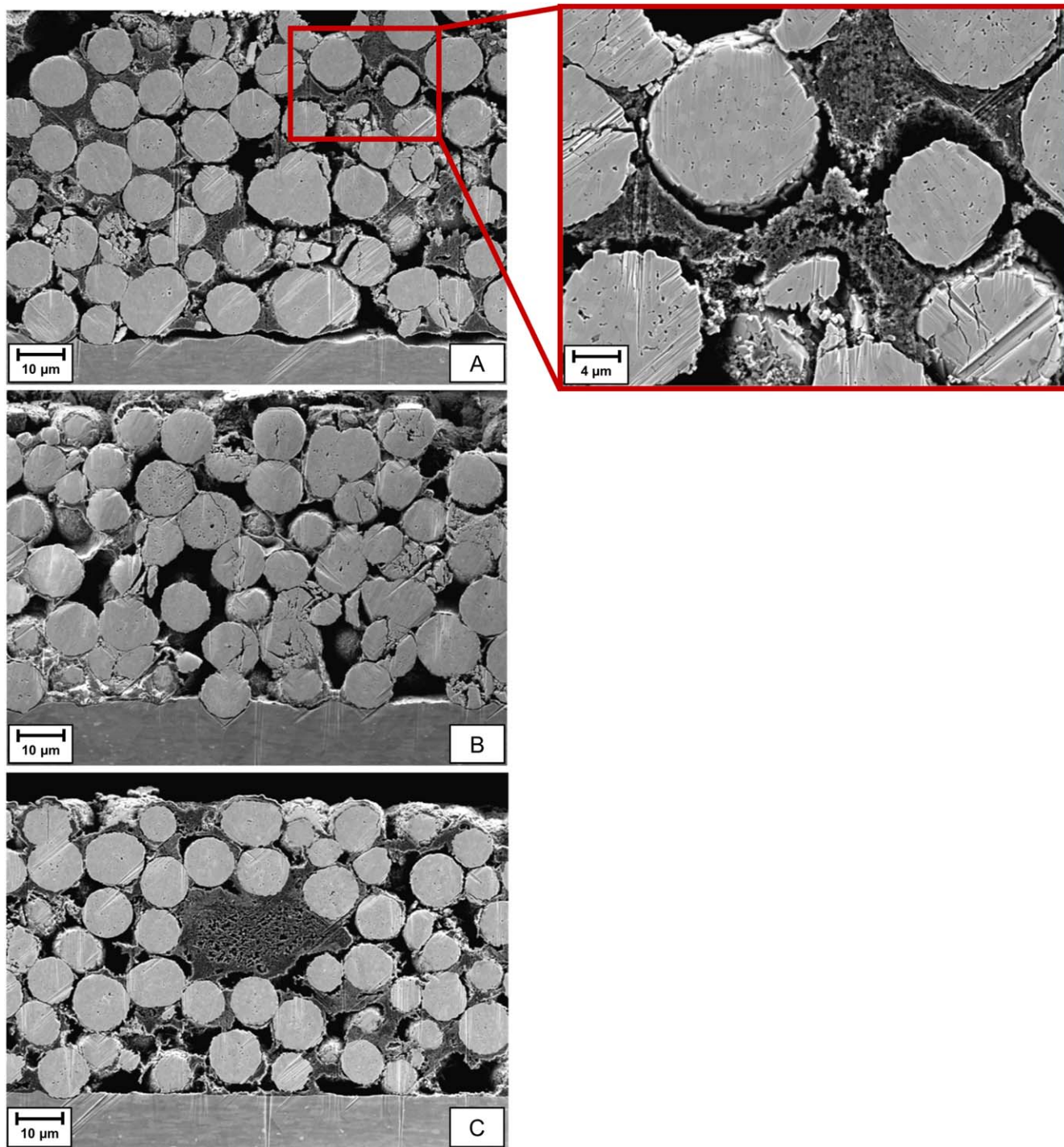


Figure 5. SEM micrographs of ion-milled cross sections of (A) C65_{2.8wt%}, (B) C65_{50.0wt%} and (C) C65/VGCF_{1.4+1.4wt%} (left) and a higher magnification of C65_{2.8wt%} showing the lack of interaction between LNMO and CBDs (right).

that delamination of the cathode coating from the current collector or the reduction of contact points between the CBDs and LNMO induced by volume changes during cycling is the responsible factor behind the observed capacity loss.²⁶ Even at the applied discharge C-rate of 1 C, charge transfer is impeded by the loss in contact points or delamination to an extent that charging cannot be completed in time. However, at lower C-rates the time for charge transfer through the remaining contact points is sufficient, resulting in a higher capacity retention.^{58–61}

Comparing the shifts in charge and discharge potentials for cycles 250, 500, 750 and 1000 as illustrated in Fig. 9, cathode

C65_{2.8wt%} containing only C65 as CA displays a significant increase in polarization, further proving delamination as the main cause for loss of discharge capacity because it leads to incomplete charging and discharging as the coatings move out of the charging window of 3.5 V–4.9 V. This can be compensated to some extent by a CV step in the charge protocol, however not completely. Interestingly, Sahore et al.²⁶ demonstrated the same degradation mechanism in their work on NMC811 when applying a combination of CMC and PVDF latex as binder system.

Even so, a rise in polarization can also be observed for electrode C65_{1.4wt%} containing only C65 as CA. This is attributed to the

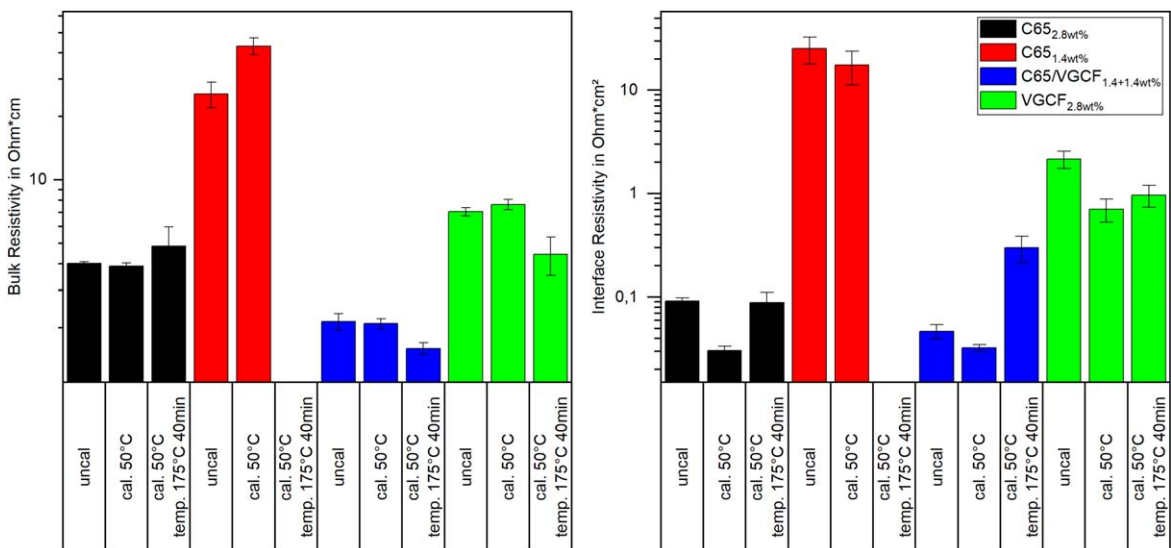


Figure 6. Bulk (left) and interface (left) resistivity of uncalendered, calendared and annealed cathodes with standard deviation, n = 5.

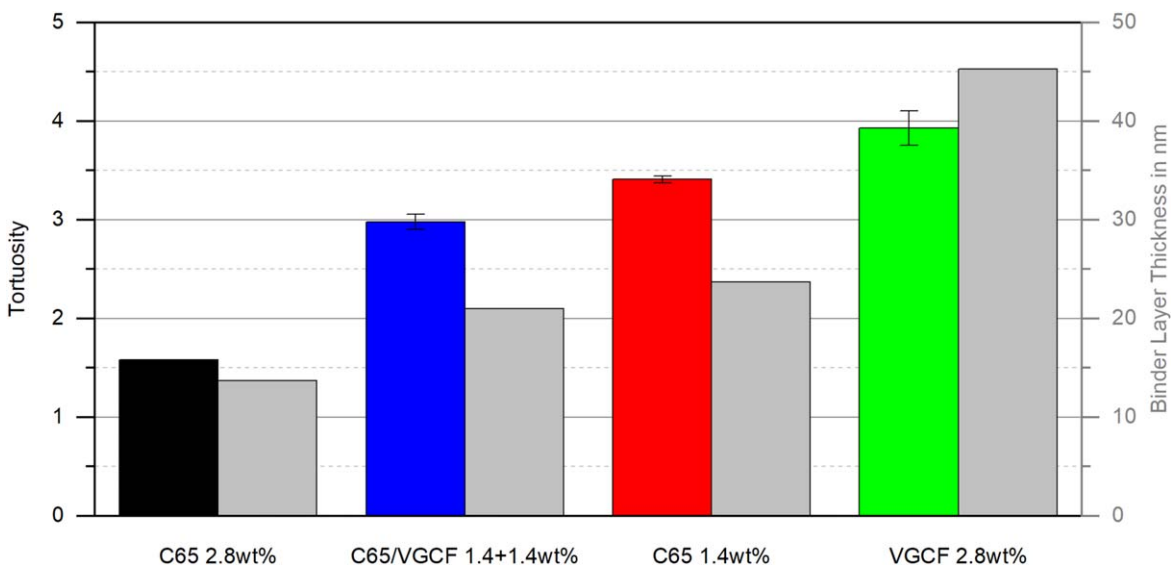


Figure 7. Tortuosity of cathodes after calendaring and annealing for 40 min at 175 °C in relation to theoretical binder layer thickness with standard deviation, n = 3.

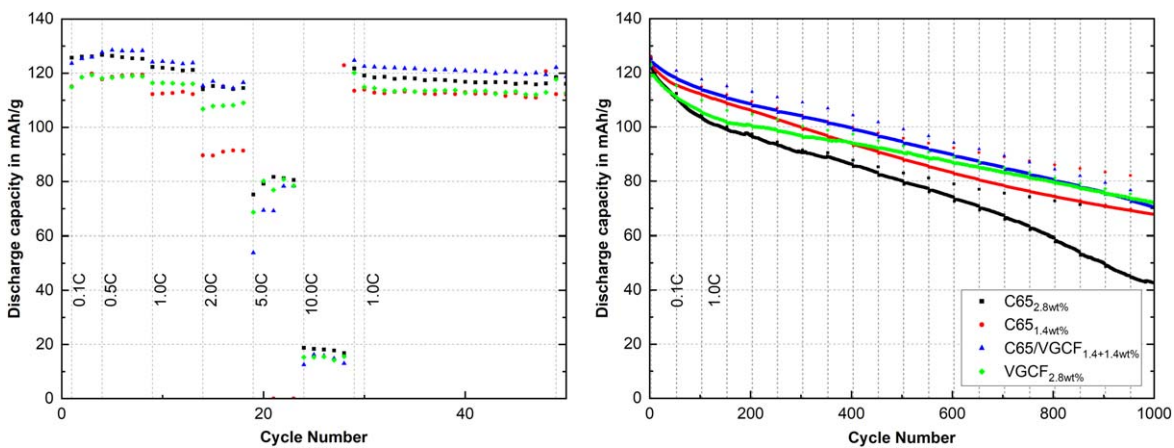


Figure 8. Rate capability (left) and long-term cycling (right) of cathodes containing different conductive additives in full cell configuration.

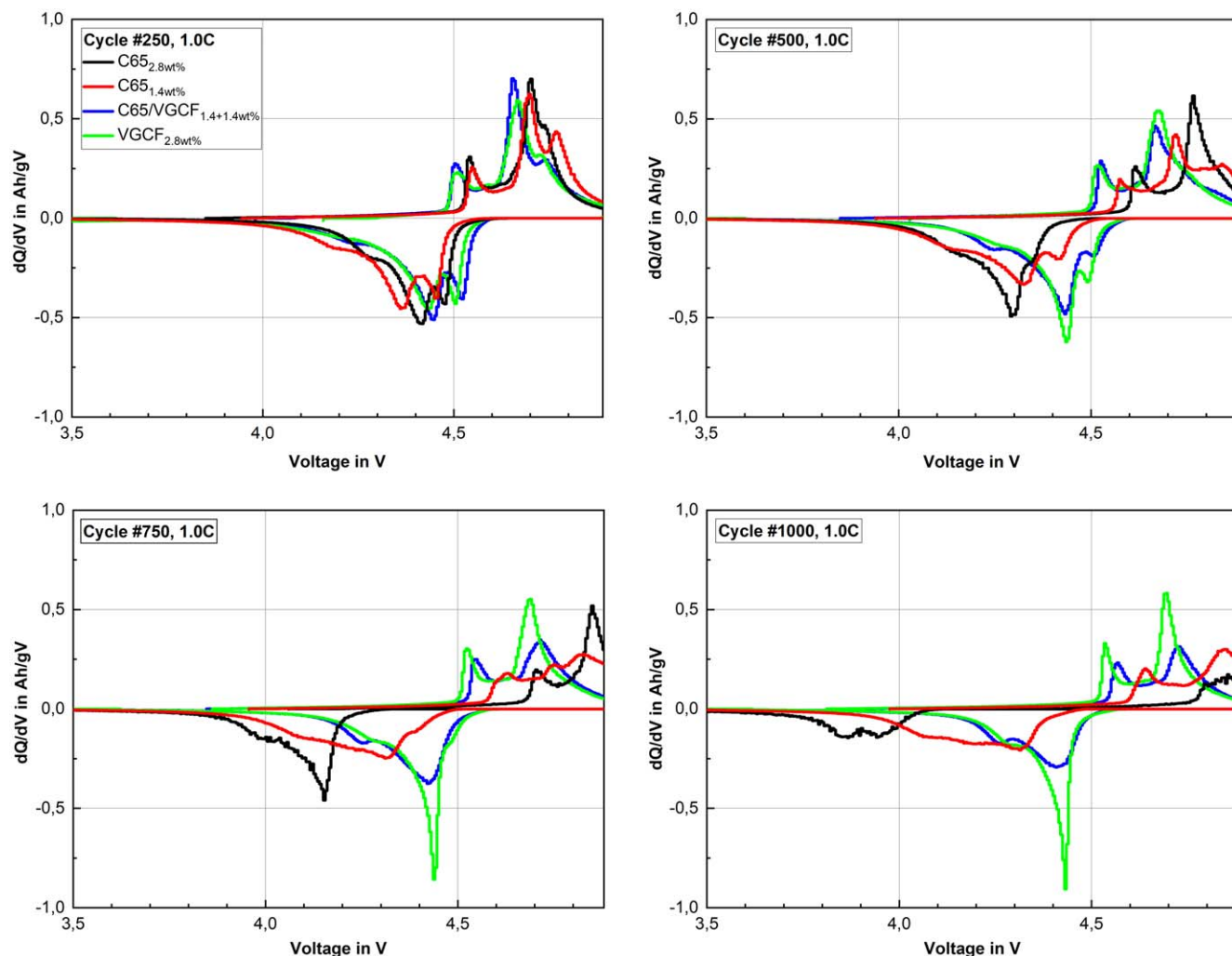


Figure 9. Differential capacity curves of cycles 250, 500, 750 and 1000.

instability of LP30 and C65 at high potentials as demonstrated by several authors and as a result the advancing deterioration of the conductive network inside the cathodes.^{17–21} For cathode C65/VGCF_{1.4+1.4wt%} a lesser degree of polarization can be observed. Due to their smaller surface area VGCFs provide fewer reaction sites for parasitic oxidation of the electrolyte leading to less hydrogen fluoride generation and therefore less damage to the cathode.^{19,21,62} Simultaneously, the long-range conductivity of the VGCFs compensates for the loss of electrical conductivity associated with the oxidation of the C65 to CO and CO₂.²¹ Cathode VGCF_{2.8wt%} demonstrates a negligible change in polarization over the course of 1000 cycles, indicating loss of lithium inventory as well as loss of active material to be the leading factors for capacity loss.^{59–61}

Conclusions

In this work, we demonstrated the utilization of two surface characterization methods (Washburn method and Sessile Drop method) for understanding and improving mechanical integrity and explaining binder distribution in aqueously processed LNMO cathodes. The techniques allow rapid surface free energy analysis of both powders and solid surfaces. Through the obtained information, one of the main driving forces in binder distribution, the interfacial free energy of adhesion, could be calculated for each relation between two electrode constituents. While surface chemistry causes preferential adhesion of the polymeric binders towards the CA, it could be shown that there are two possible solutions to improve the mechanical strength of aqueously processed cathodes.

The first and most effective one being the reduction of the CA's surface area as unbound polymer domains will become available with saturation of the CA surface.^{46,52}

Secondly, the application of VGCFs exhibiting a lower affinity towards the binders also demonstrated to be an adequate way of improving adhesion strength. Whilst the exact threshold of sufficient mechanical integrity regarding long-term cycling has not been investigated, all of the applied methods proved the successful elimination of capacity loss due to delamination from the CC.

Adjusting the surface chemistry of the binders to result in a highly negative value for the interfacial free energy of adhesion towards the active material and a less negative value with the CA is a possible next step to be pursued. Additionally, with the understanding of the principle behind binder distribution in aqueously processed cathodes, the possibility of beneficially influencing electrode tortuosity, provided the electrical resistivity is sufficiently low to not be the limiting factor, represents an interesting next field of research. Furthermore, the improvements in mechanical integrity now provide a crucial prerequisite for the manufacturing of sturdy high-loading (>3.7 mAh/cm²) cathodes.

Acknowledgments

The author wishes to acknowledge Arkema France SA for supplying the PVDF latex binder and for providing a financial support of this work. The author also thanks Francois Beaume and Gregory Schmidt of Arkema for the many fruitful discussions. This work contributes to the research performed at CELEST (Center for

Electrochemical Energy Storage Ulm-Karlsruhe). A.W. carried out the experimental work and wrote the manuscript. N.K. and A.G. contributed to the conceptualization and review. M.M. performed SEM characterizations. F.C. aided in the experimental work. W.B. and H.E. supervised the project and contributed to interpreting the findings and the revision of the final manuscript. There are no conflicts to declare.

ORCID

Andreas Weber  <https://orcid.org/0009-0008-4104-0961>
 Noah Keim  <https://orcid.org/0000-0002-3338-5811>
 Andreas Gyulai  <https://orcid.org/0000-0001-7670-4096>
 Marcus Müller  <https://orcid.org/0000-0002-5562-7201>
 Francesco Colombo  <https://orcid.org/0009-0006-4811-0091>
 Werner Bauer  <https://orcid.org/0000-0002-5923-2426>
 Helmut Ehrenberg  <https://orcid.org/0000-0002-5134-7130>

References

- Y. Liu, R. Zhang, J. Wang, and Y. Wang, "Perspective current and future lithium-ion battery manufacturing," *iScience*, **24**, 102332 (2021).
- B. Lestriez, "Functions of polymers in composite electrodes of lithium ion batteries," *Comptes Rendus Chimie. Elsevier Masson SAS*, **13**(11), 1341 (2010).
- N. Wang, Y. NuLi, S. Su, J. Yang, and J. Wang, "Effects of binders on the electrochemical performance of rechargeable magnesium batteries," *J. Power Sources*, **341**, 219 (2017).
- S. H. Sung, S. Kim, J. H. Park, J. D. Park, and K. H. Ahn, "Role of PVDF in Rheology and microstructure of NCM cathode slurries for lithium-ion battery," *Materials*, **13**, 4544 (2020).
- D. Bresser, D. Buchholz, A. Moretti, A. Varzi, and S. Passerini, "Alternative binders for sustainable electrochemical energy storage—the transition to aqueous electrode processing and bio-derived polymers," *Energy Environ. Sci.*, **11**, 3096 (2018).
- D. L. Wood, J. D. Quass, J. Li, S. Ahmed, D. Ventola, and C. Daniel, "Technical and economic analysis of solvent-based lithium-ion electrode drying with water and NMP," *Drying Technol.*, **36**, 234 (2018).
- M. Bichon, D. Sotta, E. De Vito, W. Porcher, and B. Lestriez, "Performance and ageing behavior of water-processed LiNi_{0.5}Mn_{0.3}Co_{0.2}O₂/graphite lithium-ion cells," *J. Power Sources*, **483**, 229097 (2021).
- J. He et al., "Surface structure evolution and its impact on the electrochemical performances of aqueous-processed high-voltage spinel LiNi_{0.5}Mn_{1.5}O₄ cathodes in lithium-ion batteries," *Adv. Funct. Mater.*, **32**, 2207937 (2022).
- M. Kuenzel, D. Bresser, T. Diemant, D. V. Carvalho, G. T. Kim, R. J. Behm, and S. Passerini, "Complementary strategies toward the aqueous processing of high-voltage LiNi_{0.5}Mn_{1.5}O₄ lithium-ion cathodes," *ChemSusChem*, **11**, 562 (2018).
- W. B. Hawley, A. Parejija, Y. Bai, H. M. Meyer, D. L. Wood, and J. Li, "Lithium and transition metal dissolution due to aqueous processing in lithium-ion battery cathode active materials," *J. Power Sources*, **466**, 228315 (2020).
- A. Kazzazi, D. Bresser, A. Birrozzi, J. Von Zamory, M. Hekmatfar, and S. Passerini, "Comparative analysis of aqueous binders for high-energy Li-Rich NMC as a lithium-ion cathode and the impact of adding phosphoric acid," *ACS Appl. Mater. Interfaces*, **10**, 17214 (2018).
- A. R. Schuer, M. Kuenzel, S. Yang, M. Kosfeld, F. Mueller, S. Passerini, and D. Bresser, "Diagnosis tools for humidity-born surface contaminants on Li [Ni_{0.8}Mn_{0.1}Co_{0.1}O₂] cathode materials for lithium batteries," *J. Power Sources*, **525**, 231111 (2022).
- A. M. Pillai, P. S. Salini, B. John, and M. T. Devassy, "Aqueous binders for cathodes: a lodestar for greener lithium ion cells," *Energy Fuels* (American Chemical Society, Washington, DC) (2022).
- T. F. Yi, J. Mei, and Y. R. Zhu, "Key strategies for enhancing the cycling stability and rate capacity of LiNi_{0.5}Mn_{1.5}O₄ as high-voltage cathode materials for high power lithium-ion batteries," *J. Power Sources*, **316**, 85 (2016).
- M. Armand et al., "Lithium-ion batteries—current state of the art and anticipated developments," *J. Power Sources*, **479**, 228708 (2020).
- C. Fink Elkjaer and J. Højberg, (2021), Technical Status for Haldor Topsoe LNMO Material TBM-129 High-Voltage LNMO Spinel Material (accessed 2023-10-16) www.topsoe.com/processes/battery-materials.
- J. Demeaux, M. Caillon-Caravani, H. Galiano, D. Lemordant, and B. Claude-Montigny, "LiNi_{0.4}Mn_{1.6}O₄/Electrolyte and carbon black/electrolyte high voltage interfaces: to evidence the chemical and electronic contributions of the solvent on the cathode-electrolyte interface formation," *J. Electrochem. Soc.*, **159**, A1880 (2012).
- J. Syzdek, M. Marcinek, and R. Kostecki, "Electrochemical activity of carbon blacks in LiPF₆-based organic electrolytes," *J. Power Sources*, **245**, 739 (2014).
- W. Yao et al., "A 5 V-class cobalt-free battery cathode with high loading enabled by dry coating," *Energy Environ. Sci.*, **16**, 1620 (2023).
- M. Metzger, J. Sicklinger, D. Haering, C. Kavakli, C. Stinner, C. Marino, and H. A. Gasteiger, "Carbon coating stability on high-voltage cathode materials in H₂O-free and H₂O-containing electrolyte," *J. Electrochem. Soc.*, **162**, A1227 (2015).
- M. Metzger, C. Marino, J. Sicklinger, D. Haering, and H. A. Gasteiger, "Anodic oxidation of conductive carbon and ethylene carbonate in high-voltage li-ion batteries quantified by on-line electrochemical mass spectrometry," *J. Electrochem. Soc.*, **162**, A1123 (2015).
- J. Liang et al., "Insight into prolonged cycling life of 4 V all-solid-state polymer batteries by a high-voltage stable binder," *Adv. Energy Mater.*, **11**, 202455 (2021).
- G. D. Salián, J. Højberg, C. Fink Elkjaer, Y. Tesfamhret, G. Hernández, M. J. Lacey, and R. Younesi, "Investigation of water-soluble binders for LiNi_{0.5}Mn_{1.5}O₄-based full cells," *ChemistryOpen*, **11**, e202200065 (2022).
- W. Porcher, B. Lestriez, S. Jouanneau, and D. Guyomard, "Design of aqueous processed thick LiFePO₄[Sub 4] composite electrodes for high-energy lithium battery," *J. Electrochem. Soc.*, **156**, A133 (2009).
- L. Ibing, T. Gallasch, P. Schneider, P. Niehoff, A. Hintennach, M. Winter, and F. M. Schappacher, "Towards water based ultra-thick li ion battery electrodes—a binder approach," *J. Power Sources*, **423**, 183 (2019).
- R. Sahore, M. Wood, A. Kukay, Z. Du, K. M. Livingston, D. L. W. Iii, and J. Li, "Performance of different water-based binder formulations for Ni-Rich cathodes evaluated in LiNi_{0.8}Mn_{0.1}Co_{0.1}O₂/graphite pouch cells," *J. Electrochem. Soc.*, **169**, 040567 (2022).
- J. T. Lee, Y. J. Chu, X. W. Peng, F. M. Wang, C. R. Yang, and C. C. Li, "A novel and efficient water-based composite binder for LiCoO₂ cathodes in lithium-ion batteries," *J. Power Sources*, **173**, 985 (2007).
- L. Romoli, A. H. A. Lutey, and G. Lazzini, "Laser texturing of li-ion battery electrode current collectors for improved active layer interface adhesion," *CIRP Ann.*, **71**, 481 (2022).
- K. Kierzek, "Influence of binder adhesion ability on the performance of silicon/carbon composite as li-ion battery anode," *J. Mater. Eng. Perform.*, **25**, 2326 (2016).
- F. Jeschull, D. Brandell, M. Wohlfahrt-Mehrens, and M. Memm, "Water-soluble binders for lithium-ion battery graphite electrodes: slurry rheology, coating adhesion, and electrochemical performance," *Energy Technology*, **5**, 2108–2118 (2017).
- P. G. de Gennes, "Wetting: statics and dynamics," *Rev. Mod. Phys.*, **57**, 827 (1985).
- A. Pekarovicova and P. D. Fleming, *Innovations in Ink on Paper Technology to Improve Printability* (Pira International, Leatherhead) 59–69 (2005).
- B. J. Carroll, "Physical aspects of detergency," *Colloids Surf A Physicochem Eng Asp*, **74**, 131 (1993).
- A. W. Adamson and A. P. Gast, *Physical Chemistry of Surfaces* (Interscience Publishers, New York) Vol. 150 (1967).
- S. Abbott, *Adhesion Science: Principles and Practice* (DEStech Publications, Lancaster) (2015).
- E. W. Washburn, "The dynamics of capillary flow," *Phys. Rev.*, **17**, 273 (1921).
- DataPhysics Instruments GmbH, (2023), Technical Note - Determining the Surface Energy of Powders via Washburn Method www.dataphysics-instruments.com/Downloads/ApplicationNote-DCAT-Washburn-method-Surface-energy-of-powders.pdf.
- L. Susana, F. Campaci, and A. C. Santomaso, "Wettability of mineral and metallic powders: applicability and limitations of sessile drop method and Washburn's technique," *Powder Technol.*, **226**, 68 (2012).
- F. Bashworth and J. C. Adams, *An Attempt to Test the Theories of Capillary Action* 1st ed.(University Press, Cambridge) (1883).
- Krüß GmbH, (2014), Krüss LabDesk Library Package Build 3.2.2.3064.
- D. W. van Krevelen and K. Te Nijenhuis, *Properties of Polymers*, ed. D. W. Van Krevelen and K. Te Nijenhuis (Elsevier, Amsterdam) 4th ed. (2009).
- C. Meyer, M. Weyhe, W. Haselrieder, and A. Kwade, "Heated calendaring of cathodes for lithium-ion batteries with varied carbon black and binder contents," *Energy Technology*, **8**, 1900175 (2020).
- D. K. Owens and R. C. Wendt, "Estimation of the surface free energy of polymers," *J. Appl. Polym. Sci.*, **13**, 1741 (1969).
- D. H. Kaelble, "Dispersion-polar surface tension properties of organic solids," *J. Adhes.*, **2**, 66 (1970).
- W. Rabel, "Einige Aspekte der Benetzungstheorie und ihre Anwendung auf die Untersuchung und Veränderung der Oberflächeneigenschaften von Polymeren," *Farbe und Lack*, **77**, 997 (1971).
- H. F. Wang, T. Troxler, A. G. Yeh, and H. L. Dai, "Adsorption at a carbon black microparticle surface in aqueous colloids probed by optical second-harmonic generation," *J. Phys. Chem. C*, **111**, 8708 (2007).
- M. Mezgebe, Q. Shen, J. Y. Zhang, and Y. W. Zhao, "Liquid adsorption behavior and surface properties of carbon blacks," *Colloids Surf A Physicochem Eng Asp*, **403**, 25 (2012).
- Krüß GmbH, (1999), Technical Note 306e - Models for Surface Free Energy Calculation.
- B. Ludwig, Z. Zheng, W. Shou, Y. Wang, and H. Pan, "Solvent-free manufacturing of electrodes for lithium-ion batteries," *Sci. Rep.*, **6**, 23150 (2016).
- C. J. van Oss, J. Visser, D. R. Absolom, S. N. Omenyi, and A. W. Neumann, "The concept of negative hamaker coefficients. II. Thermodynamics, experimental evidence and applications," *Adv. Colloid Interface Sci.*, **18**, 133 (1983).
- C. J. van Oss, *Interfacial Forces in Aqueous Media* (CRC Press, Boca Raton, FL) 2nd ed. (2006).
- M. K. Chaudhury, *Interfacial Interaction between Low-Energy Surfaces*, **16**, 97 (1996).
- C. C. Li and Y. W. Wang, "Importance of binder compositions to the dispersion and electrochemical properties of water-based LiCoO₂ cathodes," *J. Power Sources*, **227**, 204 (2013).
- I. Srivastava, D. S. Bolintineanu, J. B. Lechman, and S. A. Roberts, "Controlling binder adhesion to impact electrode mesostructures and transport," *ACS Appl. Mater. Interfaces*, **12**, 34919 (2020).

55. G. Liu, H. Zheng, S. Kim, Y. Deng, A. M. Minor, X. Song, and V. S. Battaglia, "Effects of various conductive additive and polymeric binder contents on the performance of a lithium-ion composite cathode." *J. Electrochem. Soc.*, **155**, A887 (2008).
56. B. Ludwig, H. Pan, J. Liu, Z. Zheng, and Y. Wang, "Powder-based additive manufacturing of li-ion batteries and micropowder mixing characteristics." *Proceedings of the ASME 2017 12th International Manufacturing Science and Engineering Conference* (2017) MSEC2017-2900.
57. C.-C. Li and Y.-W. Wang, "Binder distributions in water-based and organic-based LiCoO₂ electrode sheets and their effects on cell performance." *J. Electrochem. Soc.*, **158**, A1361 (2011).
58. V. Z. Barsykov and V. G. Khomenko, "The influence of polymer binders on the performance of cathodes for lithium-ion batteries." *Scientific Journal of Riga Technical University*, **21**, 67 (2001).
59. B. L. Trembacki, A. N. Mistry, D. R. Noble, M. E. Ferraro, P. P. Mukherjee, and S. A. Roberts, "Editors' choice—mesoscale analysis of conductive binder domain morphology in lithium-ion battery electrodes." *J. Electrochem. Soc.*, **165**, E725 (2018).
60. J. Landesfeind, A. Eldiven, and H. A. Gasteiger, "Influence of the binder on lithium ion battery electrode tortuosity and performance." *J. Electrochem. Soc.*, **165**, A1122 (2018).
61. J. Hu, Y. Wang, D. Li, and Y.-T. Cheng, "Effects of adhesion and cohesion on the electrochemical performance and durability of silicon composite electrodes." *J. Power Sources*, **397**, 223 (2018).
62. L. Spitthoff, P. J. S. Vie, M. S. Wahl, J. Wind, and O. S. Burheim, "Incremental capacity analysis (DQ/DV) as a tool for analysing the effect of ambient temperature and mechanical clamping on degradation." *J. Electroanal. Chem.*, **944**, 117627 (2023).
63. J. Zhu et al., "Investigation of lithium-ion battery degradation mechanisms by combining differential voltage analysis and alternating current impedance." *J. Power Sources*, **448**, 227575 (2020).
64. BioLogic SAS, (2023), Investigating battery aging using Differential Capacity Analysis (DCA) (accessed 2023-10-24) www.biologic.net/topics/investigating-battery-ageing-using-differential-capacity-analysis-dca.
65. Y. Li, W. Li, R. Shimizu, D. Cheng, H. N. Nguyen, J. Paulsen, S. Kumakura, M. Zhang, and Y. S. Meng, "Elucidating the effect of borate additive in high-voltage electrolyte for li-rich layered oxide materials." *Adv. Energy Mater.*, **12**, 2103033 (2022).